Separation Performance Predictions of a Stairmand High-Efficiency Cyclone

J. J. Derksen
Kramers Laboratorium voor Fysische Technologie, Delft University of Technology,
Prins Bernhardlaan 6, 2628 BW Delft, The Netherlands

Large-eddy simulations (LES) were performed on the gas flow in a Stairmand high-efficiency cyclone at Re = 280,000. The LES realistically represent the 3-D, time-dependent flow, including phenomena such as vortex core precession, and vortex breakdown. Quantitatively good agreement with measured velocity profiles is observed, for both the time-averaged velocities and the velocity fluctuation levels. The single-phase LES formed the starting point for modeling solid particle motion in the cyclone based on one-way coupling between the gas flow and the particles. It is shown that some details of the flow in the relatively small region in the vicinity of the inlet have strong influence on the separation process. Due to the long residence times of particles inside the cyclone, the concurrent simulation of gas flow and particle motion is a lengthy computational process. Therefore, three alternative ways of modeling particle motion were explored: a frozen-field approach, an eddy-lifetime model, and a periodic-flow approach. The results of these approaches are compared to the results of the concurrent simulation.

Introduction

CFD-based predictions on the performance of gas cyclones date back to 1982 (Boysan et al., 1982), that is, the early days of numerical simulation of turbulent fluid flow. The idea was (and is) that once we have a reliable prediction of the flow field in the cyclone, particle-tracking leads the way to estimates of the collection efficiency. Ultimately, the goal is to scale up, improve, or even design cyclones based on numerical modeling. Various approximations and modeling assumptions need to be adopted in order to make this flow system involving the combined transport of gas and solids tractable for numerical simulation. In many numerical studies, a one-way coupling between the gas-flow field and particle motion is assumed and particle-particle collision are discarded, although it is known from practice that the solids loading influences separation performance (Ontko, 1996; Hoffmann et al., 1992). The size of the equipment, and high throughput, makes turbulence modeling necessary. Results of the application of turbulence models based on the Reynolds-averaged Navier-Stokes (RANS) equations to cyclonic flow (or more generally strongly swirling flow) have learned that Reynolds stress models need to be applied to capture the most important aspects of the average flow field (Hoekstra et al., 1999; Spall and Ashby, 2000). Accurate predictions with respect to the flow's fluctuations are very difficult to get and most likely require very fine grids. Additional modeling is required if one wants to track solid particles in the RANS flow field, since the particles will not only feel the average velocity field, but also will get dispersed by the action of turbulence. Finally, many modeling attempts have considered the flow in the cyclone to be axi-symmetric (for example, Boysan et al., 1982; Hoekstra et al., 1999). If the cyclone is fed through a finite number of tangential inlets, this assumption is at least not valid in the entrance region for purely geometrical reasons. Furthermore, experimental observations indicate an unsteady, spiral-shape vortex core, that is, a truly three-dimensional (3-D) flow. In this contribution, some of the above mentioned modeling issues are approached along slightly alternative routes. The issues of one-way vs. two-way coupling between solids and gas and particle-particle collisions are, however, not covered. Throughout the article, one-way coupling and noncolliding particles are assumed. This simplification is not only instigated by computational considerations, but also motivated by the fact that we consider a high-efficiency cyclone. In contrast to high-throughput cyclones, high-efficiency cyclones are employed in the final stages of a separation process, when solids volume fractions have become small, and only fine particles are left in the gas stream.

The basis of our approach is a large-eddy simulation (LES) of the single-phase flow in a Stairmand high-efficiency cyclone (Stairmand, 1951) at $Re = U_{in} D/\nu = 280{,}000$ (U_{in} is the

average velocity at the inlet, D is the diameter of the body of the cyclone, and ν is the kinematic viscosity of the gas). The potential of LES for single-phase cyclonic flow has already been demonstrated by Slack et al. (2000) and Derksen and Van den Akker (2000). With our 3-D, time-dependent simulation, we have been able to accurately predict the average flow field, as well as the velocity fluctuation levels. In this time-dependent flow field, particles were released. Since, in the LES, the resolved (explicitly calculated) velocity fluctuations are much stronger than the subgrid-scale fluctuations, much less stochastic modeling of particle motion is required compared to RANS simulations. The computational burden of the concurrent simulation of gas flow and particle motion was large. This was not only because of the LES of the gas flow itself, but also because of the long time span that needed to be simulated to have the injected particles either collected or exhausted (this requires more than $200D/U_{\text{in}}$, whereas convergence of the flow statistics is typically reached after $25D/U_{\text{in}}$). For this reason, also less expensive approaches of particle transport modeling have been explored.

The first approach is borrowed from RANS modeling. The time-averaged velocity, as well as the turbulent kinetic energy field and the energy dissipation field in the whole cyclone volume as calculated with the LES, were stored (averaging time was $40D/U_{\text{in}}$). In this time-averaged field, particles obeying an eddy-lifetime model (see, for example, Boysan et al., 1982) were released, and separation efficiency was determined. In the second approach, particles were released in frozen flow fields (that is, single realizations of the simulated turbulent flow). By averaging the particle-tracking results over a few statistically independent flow realizations, average separation efficiency estimates could be obtained. In the third approach, the time dependence of the gas flow was mimicked by tracking the solid particles in a periodically played time-sequence of previously stored flow fields.

The next section is devoted to the single-phase flow. Discretization, turbulence modeling, and boundary conditions are discussed. The single-phase LES results are compared to the velocity profiles measured by Hoekstra (2000). Furthermore, the behavior of the vortex core is highlighted. Subsequently, the modeling of solid particle transport within the LES flow field will be treated. Results comprise the spatial distribution of particles within the cyclone as a function of the particle Stokes number, and grade-efficiency curves. The latter will be used to facilitate a comparison with experimental collection efficiency data. The alternative (less computationally intensive) approaches with respect to particle transport modeling are then described, followed by a summary and conclusion.

Gas-Flow Field

Modeling approach

A lattice-Boltzmann method has been used to simulate the gas flow (Chen and Doolen (1998) provide a good overview of the method). The starting point for lattice-Boltzmann schemes is a many particle system, residing on a lattice (these purely fictitious particles should not be confused with the solid particles that are used for simulating the gas-solid separation process). Every time step, the fictitious particles move to neighboring lattice sites where they collide, that is, exchange momentum with all other particles involved in the collision. This simplified kinetic model for a fluid can be constructed in such a way that the macroscopic behavior of the system resembles a real, Newtonian fluid. The specific scheme that has been used in the present work is due to Somers and Eggels (Somers, 1993; Eggels and Somers, 1995). It slightly differs from the (de facto standard) lattice BGK models (Qian et al., 1992), in the sense that it explicitly takes the third-order and some fourth-order terms into account. Subsequently, the third-order terms are effectively suppressed by the scheme making it at least second-order accurate in space and time. The major reason for employing a lattice-Boltzmann scheme is its (parallel) computational efficiency. The interactions in the lattice-Boltzmann scheme are fully localized. As a result, a distributed memory lattice-Boltzmann program based on domain decomposition only requires communication of flow variables at subdomain boundaries and, therefore, efficiently employs parallel resources. In recent publications (for example, Derksen and Van den Akker, 1999, 2000; Hollander et al., 2001) on turbulent flows in complexly shaped enclosures, we have demonstrated the large potential of lattice-Boltzmann flow simulation in chemical engineering.

The resolution of the simulations was such that one lattice spacing Δ corresponds to $D/90$. The total number of lattice cells in the simulation amounted to 7.7×10^6. A significant part of these cells (45%) lies outside the cyclone geometry. Since the lattice-Boltzmann scheme uses explicit time stepping, a CFL type of constraint limits the size of the time step. Furthermore, gas velocities need to be chosen small compared to the (finite) speed of sound in the lattice-Boltzmann scheme, which further reduces the time step. The time step that has been used in the simulations was chosen as $5.6\times10^{-4}T_{\text{int}}$ (with $T_{\text{int}} = D/U_{\text{in}}$ the integral time scale). The computer code was implemented on a Beowulf-cluster, consisting of Dual Pentium III 700 MHz PCs connected through Ethernet (100 Mbit/s). Running the fluid-flow code on six CPUs in parallel resulted in a wall clock time of 5 s per time step. The solid particle-tracking part of the code (that will be discussed below) added some 15% to the wall clock time per time step. As already indicated in the introduction, a typical single-phase simulation required some 25 integral time scales to reach statistical convergence, which corresponds to a wall clock time of 2.5 days. Due to the long residence time of solid particles in the cyclone, a concurrent simulation of fluid flow and particle motion typically took one order of magnitude longer. Total memory requirements (that is, summed up over all CPUs) were about 1.5 Gbyte.

The uniform, cubic, and (as a result) Cartesian, nature of the lattice-Boltzmann grid asked for specific attention, since we needed to implement cylindrically shaped walls. For this goal, an adaptive force field algorithm, which has been discussed in detail by Derksen and Van den Akker (1999), was employed. In the algorithm, the walls are viewed as forces acting on the fluid. Every time step, these forces are calculated in such a way that they impose a prescribed velocity (such as a zero velocity for static walls) at a large set of points that define the walls within the flow domain. These points do not necessarily need to coincide with lattice sites, and, therefore, facilitate a smooth representation of the bounding sur-

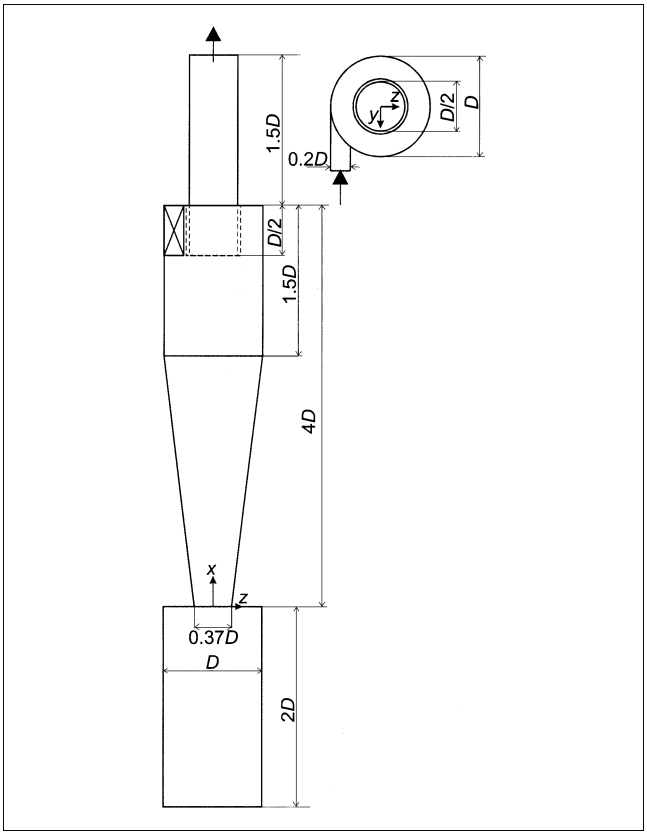

Figure 1. Flow geometry and coordinate system.

Left: side view, right: top view.

face. Second-order interpolation was used to relate velocities and forces at the lattice sites to the velocities and forces at the wall defining points.

For modeling the nonresolved scales, the standard Smagorinsky subgrid-scale model with $c_s = 0.1$ was applied (Smagorinsky, 1963). In the Smagorinsky model, the turbulent flow structures with lengthscales smaller than the grid spacing are considered to be purely diffusive, and isotropic so that they can be characterized with a local eddy-viscosity. The implementation of the Smagorinsky subgrid-scale model in the lattice-Boltzmann scheme is straightforward. In the collision phase, rather than the molecular viscosity ν, the total viscosity $\nu + \nu_e$ (with ν_e the eddy-viscosity) is used. Recently, a structure function model (Métais and Lesieur, 1992) has been implemented in our LES code. Tests on an agitated swirling flow did not show remarkable differences with the (more simple) Smagorinsky model (Derksen, 2001).

Flow geometry and boundary conditions

Figure 1 shows the flow geometry (the Stairmand high-efficiency cyclone; Stairmand, 1951), along with the definition of the coordinate system that will be used throughout the article. Swirl is generated by feeding the cyclone through a tangential inlet. Gas leaves the cyclone through the exit pipe (a.k.a. vortex finder) at the top. The bin below the conical section is used for dust collection.

For the single-phase flow, the operating conditions in the cyclone are fully determined by the Reynolds number, defined here as $Re = U_{\text{in}} D/\nu$. A value of 280,000 was adopted since that value corresponded to experimental data obtained in our laboratory by Hoekstra (2000). He achieved the latter value by letting air at ambient conditions with a superficial inlet velocity of $U_{\text{in}} = 16.1$ m/s into a cyclone with $D = 0.29$ m.

The spatial resolution of the simulations ($\Delta = D/90$) implied that the boundary layers at the no-slip walls could not be fully resolved. Wall functions were applied (Schumann, 1975). The tangential velocity at the first grid point was taken to be $10u^*$ (in accordance with Eq. 45 in Schumann (1975)), where the wall shear velocity u^* was estimated to be $0.03U_{\text{in}}$ for the entire geometry (in accordance with findings in a similar flow system reported in Derksen and Van den Akker (2000)). At the inlet area, a (laminar) parabolic velocity profile was assumed. In real life, the inlet flow is definitely not laminar (its Reynolds number is $Re_{\text{in}} = 0.2\,Re$). In the simulations, the results appeared to be insensitive to the specific inlet velocity profile: comparing the results of simulations with uniform and parabolic inlet profiles showed hardly any differences in terms of the average velocities and fluctuation levels in the body of the cyclone. This insensitivity is likely due to the virulent region where the inlet flow merges with the swirling gas already present in the body of the cyclone. In this region, the gas quickly forgets the conditions in the inflow channel. At the exit area (that is, the plane at $x = 5.5D$), a zero-gradient boundary condition was imposed ($\partial/\partial x = 0$).

Swirling flows can exhibit subcritical behavior (Escudier et al., 1982): swirl allows for the axial propagation of inertial disturbances relative to the flow. The relative speed of propagation increases with the intensity of the swirl. In the case of subcritical flow, the swirl is so strong that disturbances do not only propagate downstream, but also upstream. If in a simulation, the flow is subcritical at the location of an outflow boundary, the location and type of outflow boundary condition will (likely in an unphysical manner) influence the outcome of the simulation in the entire field, not only in the vicinity of the boundary. To prevent subcritical flow at the outflow boundary, we placed an obstruction in the exit pipe at $x/D = 4.84$, that is, slightly upstream of the outflow boundary (see Figure 2). The obstacle (a circular disk with diameter $0.36D_{\text{exit}}$ and thickness $0.14D_{\text{exit}}$) takes care of a sub- to supercritical transition (Benjamin, 1962) before the gas reaches the outflow plane. It was checked to what extent the size and exact location of the obstacle did influence the overall flow field predictions. No significant effects were observed, unless the obstacle was too small and the subcritical flow extended to the outflow plane.

Flow field results

Flow field impressions in an axially oriented plane (the x-z plane with $y = 0$, as defined in Figure 1) are given in Figure 2. In the body of the cyclone (that is, the part in between the top at $x = 4D$, and the dust collection bin at $x = 0$) the figure shows downflow near the wall and upflow near the center. Close to the vortex core, an axial velocity deficit can be observed in a large part of the cyclone body. The core has a spiral shape that extends into the dust collection bin, making the flow nonaxisymmetric. The vicinity of the inlet is highlighted in the two more detailed vector plots in Figure 2. The

snapshot demonstrates the turbulent character of the flow, whereas the average field shows two persistent recirculation regions. The first is close to the top of the cyclone body, in the annular region in between the cyclone wall and vortex finder, and the second is close to the outer wall (at the side with negative z), just below the inlet channel. It is the consequence of the abrupt ending of the bottom surface of the inlet channel, resulting in boundary layer separation. These two recirculations have a significant impact on solid particle motion inside the cyclone, as will be demonstrated in the section on particle motion. Just upstream of the vortex finder entry vortex breakdown occurs, similar to the breakdown structures observed by Escudier et al., (1980) slightly upstream or inside a contraction.

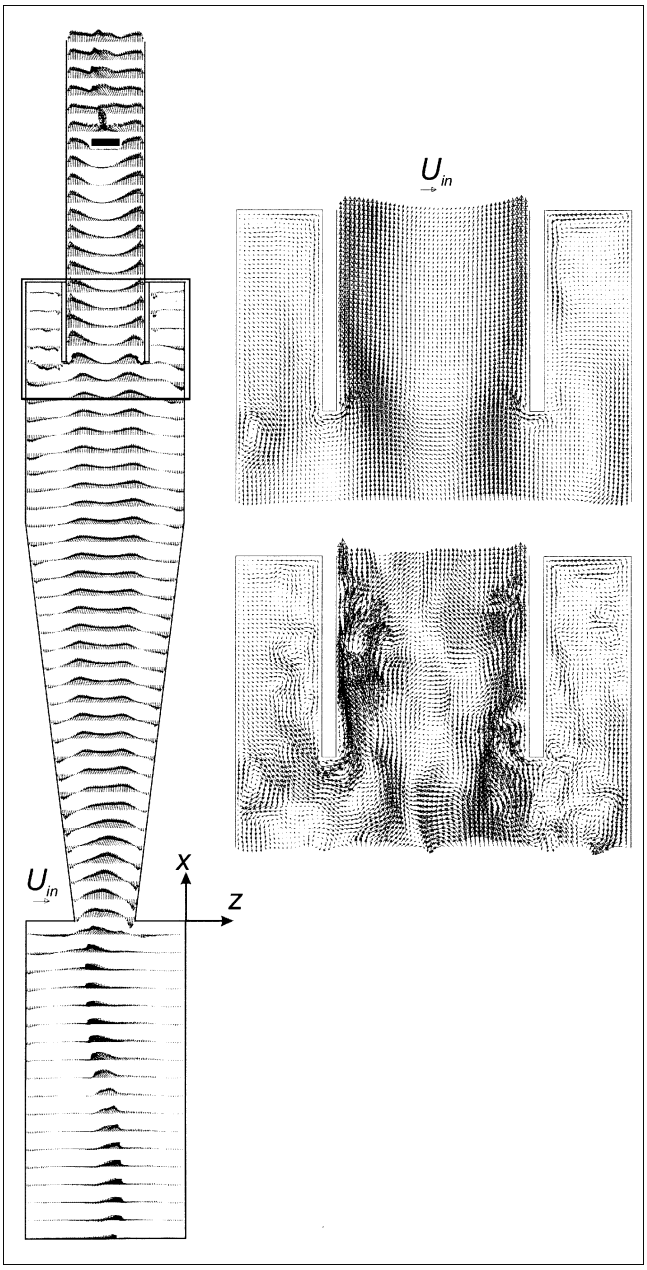

Figure 2. Flow in the $y = 0$ plane in terms of velocity vectors.

Left: the average flow in the entire plane. Note the obstruction in the exit pipe. Right-top: average flow in the inlet region (indicated with the rectangle in the left figure). Right-bottom: a single realization of the flow in the inlet region.

In Figure 3, the LES results are confronted with the experimental data (Hoekstra, 2000) that consist of velocity profiles measured by laser Doppler anemometry (LDA). At a few axial locations, the LDA measuring volume was traversed along the y-axis. The tangential and axial velocity components were measured. From the LDA data sets, time-averaged velocities and root-mean-square (RMS) values of the velocity fluctuations were extracted. Good agreement between simulation and experiment with respect to the average velocities profiles can be concluded. Details, such as the asymmetry of the axial velocity profiles in the lower part of the cyclone body (related to the spiral shape of the vortex core) are well represented by the LES.

Both experiment and LES show increased fluctuation levels near the center of the cyclone, which are caused by vortex core precession (as will be discussed in more detail below). In the center region, vortex core precession implies a relation between the gradients of the average velocity profiles, and the RMS profiles, since (as a first approximation) the fluctuations induced by vortex core precession in a point can be viewed upon as the result of the precessing motion of the average velocity profiles over that point. The experimentally determined tangential RMS profiles show a local minimum near the center, a minimum that is largely missed by the LES. In the experiments, the minimum is due to the slight decrease in the average tangential velocity gradient in the center. The latter feature is to some extent (but not fully) resolved by the LES. The consequence of this slight deviation in the average tangential velocity profile is the absence of a local minimum in the center of the simulated tangential RMS profile. Less pronounced, but similar, deviations between experiment and simulation are found for the axial RMS profiles.

It is worthwhile noticing that, in order to realistically model the flow in the cyclone, the dust collection bin definitely needs to be taken into account. In Figure 4, a few profiles of simulations without the dust collection bin (that is, a no-slip wall was placed at the end of the cone at $x = 0$) are shown. Strong deviations throughout the cyclone can be observed. The intensity of swirl in the vortex core is now clearly overestimated by the LES. This has drastic consequences for the axial velocity profiles: they become much more pronounced.

Vortex core precession was investigated by monitoring a simulated velocity time series in the center of the cyclone (see Figure 5). Some coherency (a characteristic feature of vortex core precession) in the simulated fluctuations can already be observed with the naked eye. The power spectrum derived from the LES time series confirms this observation since it shows a peak at $f_{p,\mathrm{LES}} = 1.61 U_{\mathrm{in}}/D$ (that is, the Strouhal number of the most dominant fluctuation $S = f_{p,\mathrm{LES}} D/U_{\mathrm{in}}$ amounts to 1.61). In Figure 5, the simulated temporal velocity fluctuations in a transverse (z-) direction are confronted with measured (LDA) fluctuations in the axial (x-) direction (measurements due to Hoekstra (2000)). Different velocity components are compared since in the LES only transverse velocity time series have been stored, while the

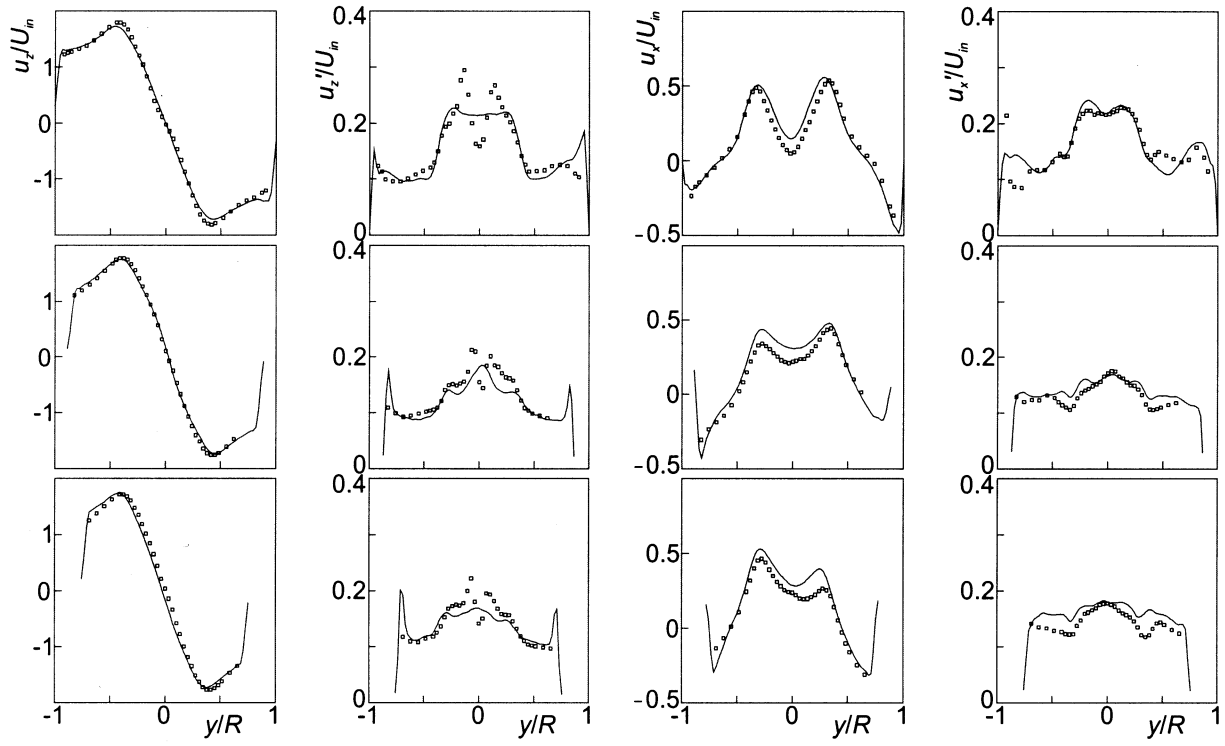

Figure 3. Velocity profiles along the *y*-axis (the position on the *y*-axis has been nondimensionalized with $R = D/2$) at three axial locations.

From top to bottom: $x = 3.25D$, $x = 2.0D$, and $x = 1.5D$. From left to right: average z-component (tangential velocity), RMS of z-component, average x-component (axial velocity), and RMS of x-component. The symbols are LDA experiments (Hoekstra, 2000), the solid lines are LES results.

data rate of the transverse velocity measurements was too low to extract a meaningful spectrum. However, the purpose of the comparison between experiment and simulation here solely is the identification of principal frequencies. If present, the same principal frequencies will pop up in the spectra of all velocity components (Hoekstra, 2000). The experimental and LES spectra show striking resemblances and differences. Next to a peak at $S = 1.58$ (that corresponds very well to the position of the LES peak), a peak at $S = 0.70$ is present in the experiments. Please note that the $S = 1.58$ peak is not just a higher harmonic of the $S = 0.70$ peak; $S = 1.58$ is a principal frequency of the flow system. It is not clear why the LES misses the frequency corresponding to $S = 0.70$.

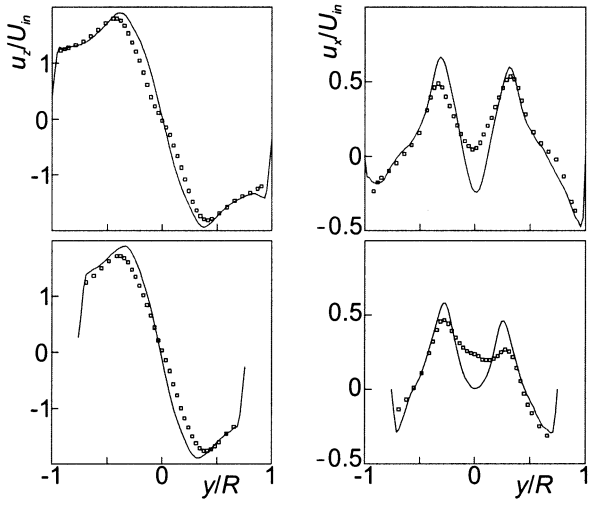

Figure 4. Drawn lines: LES velocity profiles along the *y*-axis at two axial locations: $x = 3.25D$ (top), and $x = 1.5D$ (bottom) in a cyclone without dust collection bin.

Left: average z-component; right: average x-component. The symbols are the same LDA experiments as in Figure 3 (that is, measured with the collection bin).

The time-averaged behavior of the vortex core, defined as the line connecting the points in all horizontal planes having zero horizontal velocity, is highlighted in Figures 6 and 7. Figure 6 shows that on average the core of the vortex spirals around the geometrical center of the cyclone body. The amplitude of the core's precessing motion is a pronounced function of the axial position in the cyclone (Figure 7). The sudden contractions/expansions in the geometry at $x = 0$ (the bottom of the cone), and at $x = 3.5D$ induce strong vortex motion. This also applies to the obstacle in the exit pipe (at $x = 4.84D$). Downstream of the obstacle (that is, in the supercritical region) and inside the dust collection bin, the least virulent vortex motion is observed. The amplitudes in the y and z-direction are approximately equal throughout the cyclone, indicating an isotropic precession.

For solid particle motion, next to the average velocity field, the turbulent kinetic energy field is of prime importance. In fact, the major motivation for applying LES to cyclonic flow has been that in modeling particle motion, less stochastic

modeling is required since the most energy containing eddies are resolved explicitly. The latter is demonstrated in Figure 8, where the resolved turbulent kinetic energy field, and the subgrid-scale kinetic energy field, are compared. The subgrid kinetic energy k_{sgs} has been estimated based on isotropic, local-equilibrium mixing-length reasoning according to

$$k_{sgs} = C_k c_s^2 \Delta^2 |\boldsymbol{S}|^2 \tag{1}$$

with $|\boldsymbol{S}|$ the resolved deformation rate, Δ the grid spacing, and C_k a constant amounting to 5 (Mason and Callen, 1986). Equation 1 is mainly intended to provide a diagnostic estimate for the subgrid-scale fluctuations. Close to walls, the isotropy assumption implied by Eq. 1 is clearly violated. Grossly speaking, the subgrid-scale kinetic energy is one order of magnitude lower than the grid-scale kinetic energy.

Solid Particle Motion

Model description

To numerically study the collection efficiency of the Stairmand high-efficiency cyclone, particles were released in the LES flow field. The particles were considered to be noncolliding, spherical entities that experience gravity (without buoyancy; the applications relate to gas-solid systems), and Stokes-drag. One-way coupling was assumed, albeit that mass loading effects on cyclone separation performance have been witnessed for mass loadings as low as 1% (Ontko, 1996), that is, at very low particle volume fractions (of the order of 10^{-5}).

The above assumptions imply that (given the flow geometry) the particulate flow problem is fully defined by three dimensionless numbers: the gas-flow's overall Reynolds number (Re as defined above), the particle's Stokes number [$Stk = (\rho_p/\rho_g)(d_p^2 U_{\text{in}}/18\nu D)$, with d_p the particle diameter and ρ_p/ρ_g the particle over gas density ratio], and the Froude number ($Fr = U_{\text{in}}^2/D|\boldsymbol{g}|$, with $\boldsymbol{g}$ the gravitational acceleration vector). At $Re = 280{,}000$ and $Fr = 90$ (these conditions relate to the experimental conditions of Hoekstra (2000) see also the subsection on the flow geometry and boundary conditions), 23 sets each consisting of 12,000 identical particles were tracked through the cyclone. The 23 Stokes numbers are in the range $Stk = 5\times10^{-6}$ to 0.39. The particles were released at the inlet area, where they were uniformly distributed. Feeding particles was started at $t = 0$ in a fully developed flow. At $t = 18T_{\text{int}}$, adding new particles was stopped. Every time step, the particle positions were updated according to the following equation

$$\frac{d\boldsymbol{v}_p}{dt} = \frac{U_{\text{in}}}{Stk\,D}(\boldsymbol{u} - \boldsymbol{v}_p) + \mathbf{g} \tag{2}$$

with $\boldsymbol{v}_p$ the particle velocity vector, and $\boldsymbol{u}$ the gas velocity at the location of the particle. This equation was time-dis-

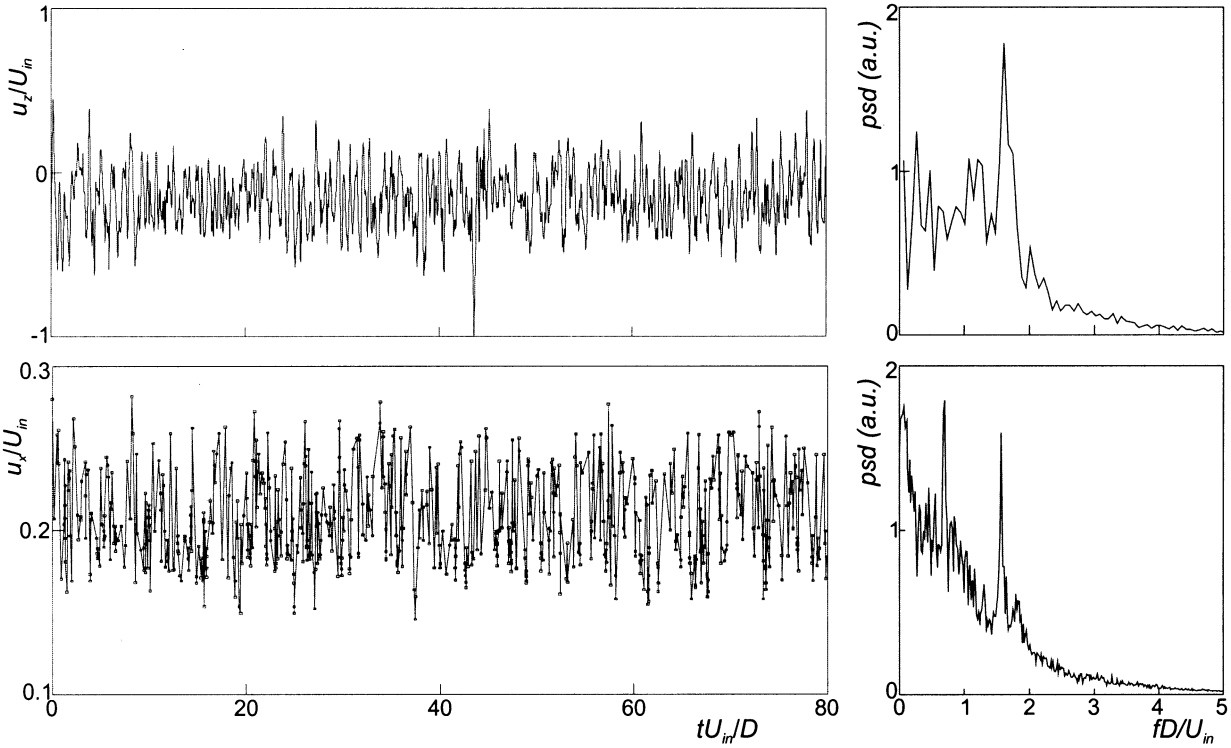

Figure 5. Temporal behavior of the velocity in the vortex core at $x = 2D$.

Top-left: part of a simulated time series of the z-velocity component at the center of the cyclone. Top-right: the power spectral density (psd) of the same time series. The psd was obtained by cutting a $224D/U_{\text{in}}$ long time series into 15 blocks, taking the FFT of each block, and then averaging the 15 psd's. Bottom-left: part of an experimental (LDA) time series of the x-velocity component at approximately the same position in the cyclone. The symbols indicate the individual velocity measurements. Bottom-right: the corresponding psd.

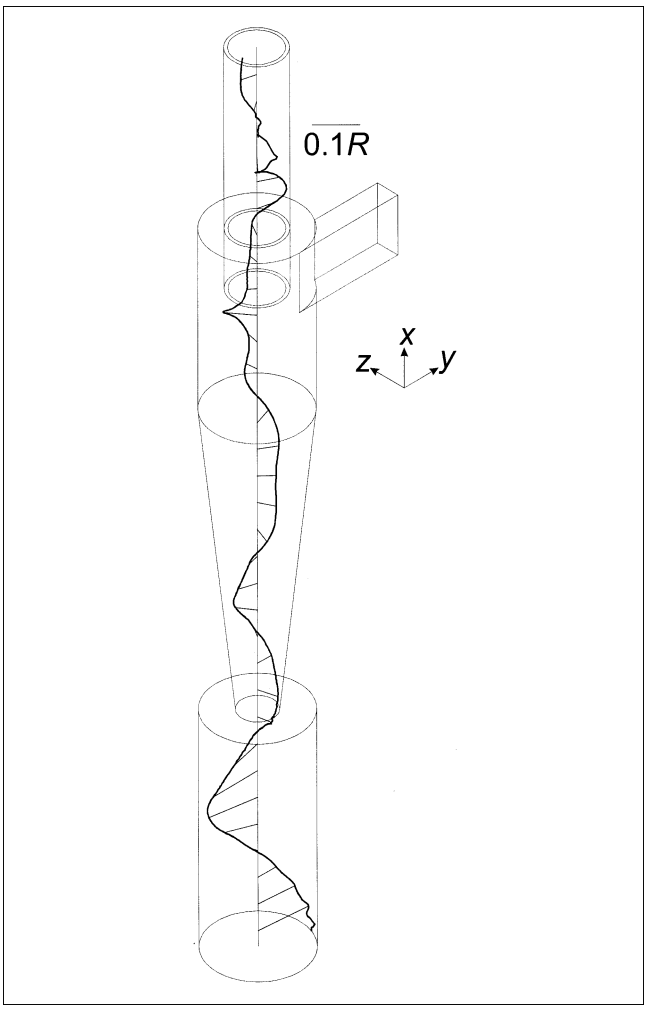

Figure 6. Time-averaged position of the vortex core in the cyclone.

Note that the deviations from the center position are not on scale.

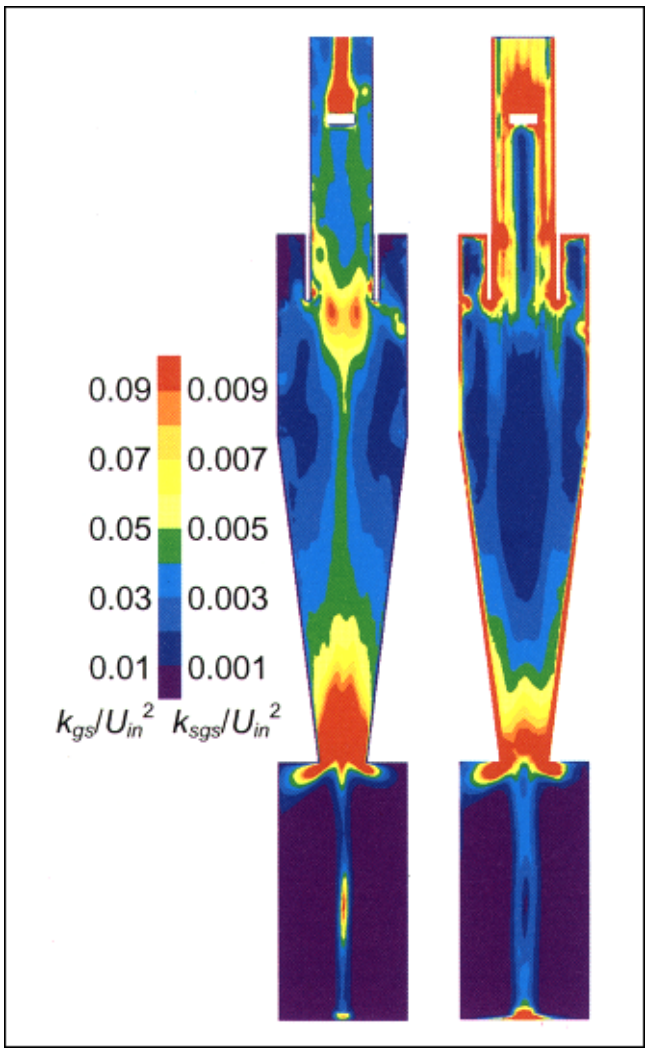

Figure 8. Grid-scale (left), and subgrid-scale (right) turbulent kinetic energy in the x-z plane at $y = 0$.

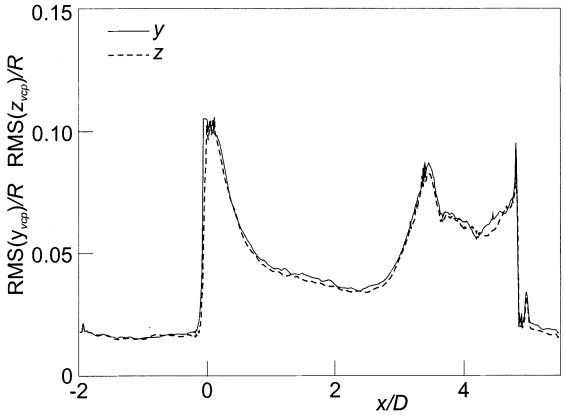

Figure 7. RMS values of the displacement in the y- and z-direction of the vortex core from its time-averaged position as a function of the axial position in the cyclone.

cretized according to an Euler-implicit scheme. Equally sized time steps were applied in the LES, and the particle update algorithm. All particle-wall collisions were considered to be fully elastic. Once a particle crossed the plane $x = 5.5D$ (the outflow boundary), it was considered to be exhausted.

In the LES, the gas velocity is composed of a resolved part, and a subgrid-scale part. The former was determined by a linear interpolation of the velocity field at the grid nodes to the particle position, and the latter is mimicked by a uniform random, isotropic process with zero average and an RMS value u_{sgs} that amounted to $u_{sgs} = \sqrt{2/3k_{sgs}}$. The subgrid-scale kinetic energy k_{sgs} was estimated with Eq. 1.

Particle motion results

Figure 9 shows the time evolution of the particle transport process. The moment $t = 18T_{\text{int}}$ corresponds to the end of the time interval during which particles were fed into the cyclone. Spiral-shape structures can be observed at the outer

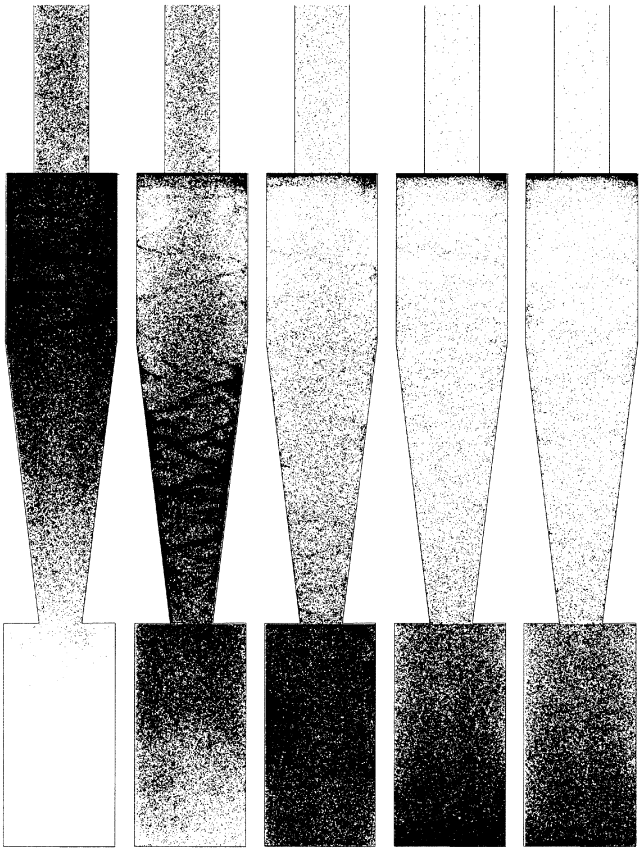

Figure 9. Side view of the cyclone with the particles at five moments in time.

From left to right: $t = 18T_{int}$, $51T_{int}$, $90T_{int}$, $152T_{int}$, and $228T_{int}$.

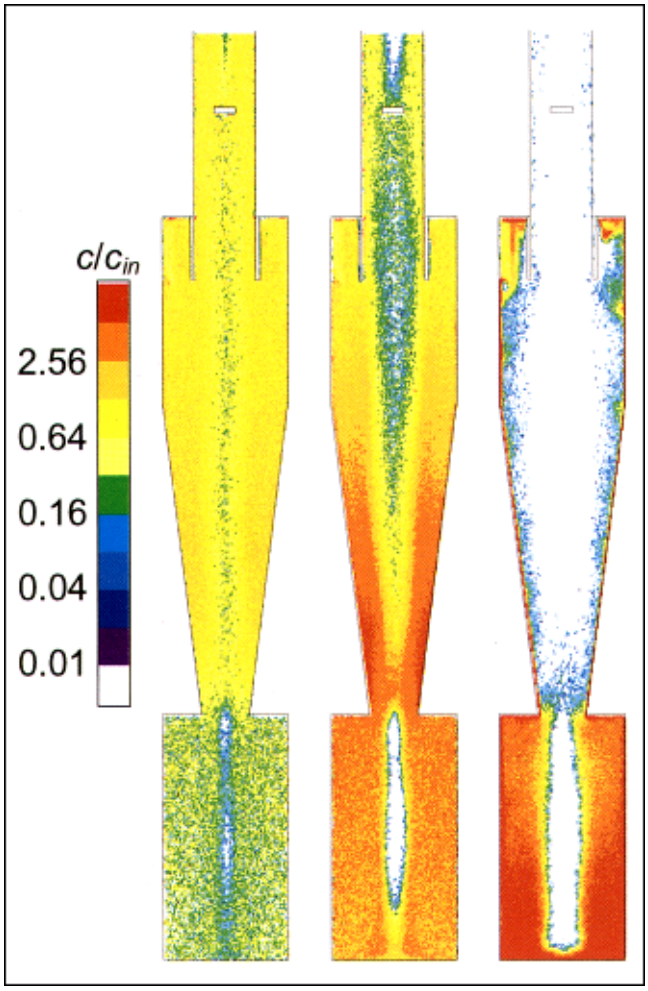

Figure 11. Time-averaged particle concentration in the x - z plane at y = 0, at three Stokes numbers.

From left to right $Stk = 6.5\times10^{-5}$, 1.4×10^{-3}, and 3.0×10^{-2}. The concentration levels have been normalized with the particle concentration at the inlet (c_{in}).

wall of the cyclone body. This feature strongly resembles observations in our transparent experimental facility. At $t = 228T_{int}$, still a considerable amount of particles has neither been exhausted, nor collected (if we define particle collection as a particle being inside the collection bin; particle collection defined this way is not definitive since it has been observed that, on some occasions, particles exit the collection bin). Most of the particles that are still inside the cyclone body are captured in the recirculation region in the annulus in between the exit pipe and the cyclone wall, near the top of the cyclone body (see Figure 2). The time-series of the fraction of exhausted particles (Figure 10) shows a trend consistent to what was observed in Figure 9: small numbers of particles are still being exhausted long after particle injection was stopped. This long-time-tail behavior of the separation process is an important issue in relation to the computational effort of the simulations.

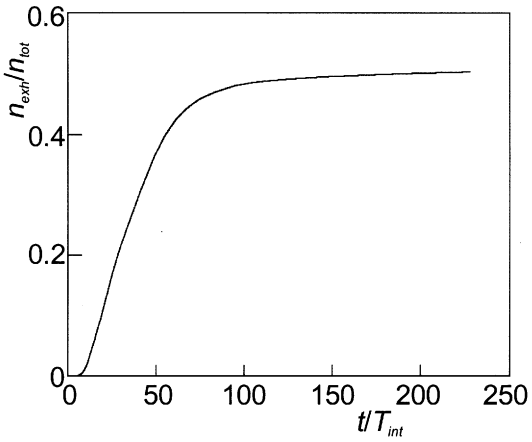

Figure 10. Fraction of exhausted particles as a function of time.

A more quantitative view on cyclone operation is given in Figure 11: the smaller particles (with the lower Stokes numbers) get dispersed in the cyclone and are then likely to be caught by the (on average upward) flow in the core of the cyclone, and exit through the vortex finder. It is interesting to see how the (bigger) particles with $Stk = 3.0\times10^{-2}$ behave in the inlet/exit-pipe region. In the inlet area, they are homogeneously dispersed as a result of the imposed inlet conditions.

They do not attach immediately to the wall once they enter the body of the cyclone, as the still bigger particles do (not shown), but have some chance to enter the weak shortcut flow that directly guides gas from the annulus in between the vortex finder and the cyclone wall into the exit pipe (see the detailed vector plots of Figure 2) and get exhausted. The recirculation due to boundary layer separation at the bottom of the inlet channel plays a prominent role in this process: its presence acts as an obstacle and enhances shortcut flow. As a result, at the side of the recirculation (the left-hand-side of the cyclones in Figure 11) relatively many particles with $Stk = 3.0\times10^{-2}$ enter the exit pipe. Also quite some particles with $Stk = 3.0\times10^{-2}$ get detached from the wall in the bottom part of the conical section due to the high turbulent activity (see Figure 8) in this part of the flow.

The collection efficiency (or grade-efficiency) curves (Figure 12) indicate a cut-size corresponding to $Stk_{50} = 1.5\times10^{-3}$ (the cut size of a cyclone is defined as the particle size that for 50% gets collected). From $t = 136T_{\text{int}}$ on, the cut-size is virtually independent of the time-span of the simulations, although, at this moment in time, 6% of the particles is still inside the body of the cyclone. These particles can be divided into two classes: big particles that have a long residence time inside the cyclone body due to their close proximity to the wall, but are collected anyhow, and particles close to the cut size that cannot decide on collection or exhaustion. Apparently, their decision does not significantly influence the collection efficiency curve anymore (compare the grade-efficiency curves at $t = 228T_{\text{int}}$, and $t = 136T_{\text{int}}$). The decrease in the collection efficiency in the low Stokes number part of the curve from $t = 136T_{\text{int}}$ to $t = 228T_{\text{int}}$ can only be explained by the fact that small particles have escaped from the dust collection bin during that time interval.

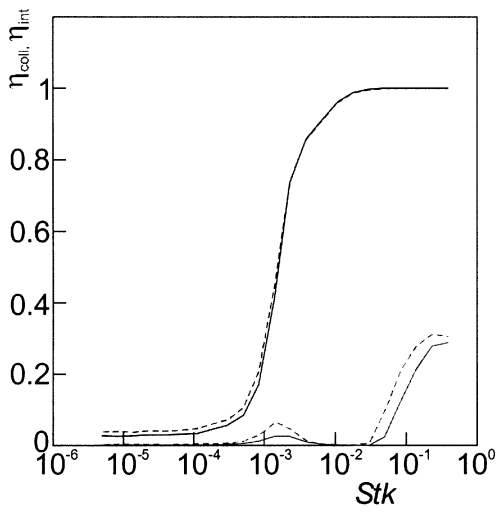

Figure 12. Two upper curves: grade-efficiency (here defined as the fraction of particles that is not exhausted) as a function of the Stokes number.

Solid line: at $t = 228T_{\text{int}}$, dashed line: at $t = 136T_{\text{int}}$. Two lower curves: fraction of particles inside the cyclone, but not in the collection bin, at the same moments in time.

Simplifying particle modeling approaches

The long time-span of the concurrent simulation of gas flow and particle motion prompted us to look into alternative ways of particle transport modeling. In the first instance, two methods were explored. In a later stage, a third alternative was added. In the first method, the time-averaged (averaging time $40T_{\text{int}}$), 3-D flow field is stored in terms of the three average velocity components, the turbulent kinetic energy (the sum of the resolved and unresolved part), and the energy-dissipation rate. The same amount of particles with the same Stokes numbers as used in the previous section now experience the average flow, and an isotropic random gas velocity with zero mean and RMS value $u' = \sqrt{2/3k}$ with k the sum of grid-scale and subgrid-scale turbulent kinetic energy. To deal with coherency in the turbulent flow, the eddy-lifetime concept has been adopted where the time interval t_{eddy} in between two updates of the random part of the gas velocity is related to a turbulent time scale: $t_{\text{eddy}} = C_L(k/\epsilon)$ (with ϵ the energy dissipation rate; the constant C_L was set to 0.15 in accordance with, for example, Boysan et al. (1982)).

In the second method, the particles are released in statistically independent flow field realizations (frozen fields). In this study we used 16 realizations, each separated $2T_{\text{int}}$ in time. In each realization, sets of particles are released and tracked through the (now static) flow. The procedure for updating the particle position is exactly the same as in the concurrent simulation of gas flow and particle motion, except that now the gas flow does not change in time. The particles still experience random fluctuations due to the subgrid-scale velocity u_{sgs}. Average particle collection properties are obtained by averaging the results of the 16 frozen fields. Compared to the concurrent simulation, the two alternative methods are very cheap in terms of computer time (they consume less than 1% of the time needed to execute the concurrent simulation), whereas they require similar amounts of computer memory.

The results for the two methods are summarized in Figures 13a, 13b and 14. In Figure 13, the particle concentration in a cross-section of the cyclone for a Stokes numbers close to Stk_{50} has been displayed. This picture should be compared to the center graph in Figure 11. In the first place, it is clear that in the frozen-field model, the particles with $Stk = 1.4\times10^{-3}$ get much better collected: high particle concentrations in the dustbin. Furthermore, particle concentrations in the core of the cyclone are highest for the concurrent simulation. A comparison between the three approaches considered so far in terms of collection efficiency shows distinct differences. The Stk_{50} of the eddy-lifetime model is almost the same as for the concurrent simulation: 1.4×10^{-3} (vs. 1.5×10^{-3} for the concurrent simulation). The shape of the grade-efficiency curve is, however, much sharper. For the small-particle tail of the curve, the eddy-lifetime model virtually predicts $\eta_{\text{coll}} = 0$, a phenomenon that is hardly ever observed in separation experiments (Cullivan et al., 2001). The shape of the frozen-field curve is similar to that of the concurrent simulation, the cut-size is, however, markedly different: $Stk_{50} = 1.1\times10^{-3}$.

An extension of the frozen-field approach in which the solid particles feel a time-varying gas-flow field has been achieved by repeatedly playing a (previously stored) time-sequence of flow field realizations. In this time-sequence particles are tracked. This method (that has been denoted the periodic-

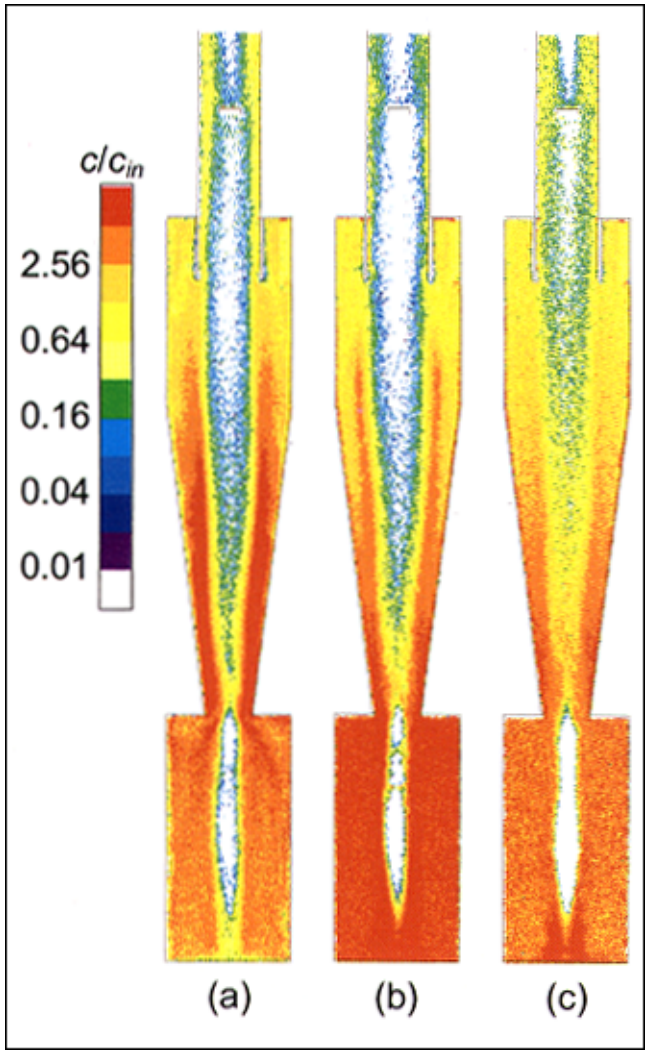

Figure 13. Time-averaged particle concentration in the *x*-*z* plane at $y = 0$ for particles with $Stk = 1.4 \times 10^{-3}$.

(a): Eddy-lifetime model, (b): frozen-field approach, (c): periodic-flow approach. The concentration levels have been normalized with the particle concentration at the inlet (c_{in}).

flow approach) will be explored here briefly. During an LES of the gas-flow field over one integral time scale, 120 flow fields have been stored on disk, representing approximately 15 Gbyte of data (in the present implementation of the periodic-flow approach, the storage capacity and the intensive i/o required are bottlenecks). Now particles are released in the cyclone. These particles feel an unsteady flow field that is linearly interpolated (in time) between the subsequent flow realizations. The sequence with which the realizations are played back is periodic: from field 1 to 120, and then back from 120 to 1 (the latter is done to avoid discontinuities in the velocity time series; it is not physically correct with a view to the gas-flow field, since, during the back sequence, the $\partial/\partial t$ term in the Navier-Stokes equation changes sign, whereas the rest of the terms remains unchanged).

We have performed the procedure for two different time-

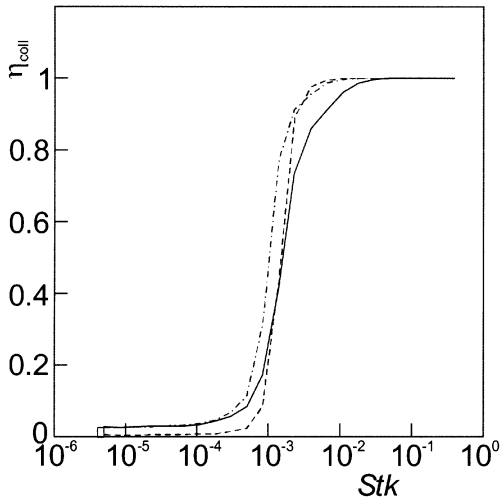

Figure 14. Grade-efficiency (here defined as the fraction of particles that is not exhausted) as a function of the Stokes number.

Solid line: concurrent simulation (same as Figure 12, solid line), dashed line: eddy-lifetime model, dash-dotted line: frozen-field model.

sequences of the gas flow, with three particle injections during each sequence. The results have been averaged over the (in total) six particle injections, and are summarized in Figure 13c and 15. Compared to the frozen-field grade-efficiency curve, the periodic-flow curve corresponds much better to the curve obtained with the concurrent simulation: apparently, the time-dependence in the flow felt by the solid particles has a significant impact on the separation process. The cut-size of the periodic-flow approach corresponds to a Stokes number $Stk_{50} = 1.4 \times 10^{-3}$, that is, close to the 1.5×10^{-3} of the concurrent simulation. However, significant dif-

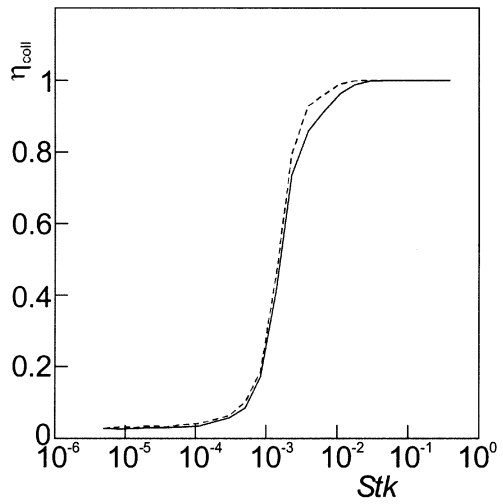

Figure 15. Grade-efficiency (here defined as the fraction of particles that is not exhausted) as a function of the Stokes number.

Solid line: concurrent simulation (same as Figure 12, solid line), dashed line: periodic-flow approach.

ferences between the two curves in Figure 15 can be observed in the part above the cut-size. A reason for these deviations could be that the time-series of flow fields that formed the basis of the periodic-flow approach were not long enough compared to the relaxation times of the larger particles. The particle concentration field for $Stk = 1.4 \times 10^{-3}$, as obtained with the periodic-flow approach (Figure 13c), is very similar to the field extracted from the concurrent simulation (center field in Figure 11).

The concurrent simulation of gas flow and particle motion has the soundest physical basis, and may, therefore, approach physical reality best. In terms of the grade-efficiency curves, the first two alternative methods deviate considerably from the concurrent simulation and, therefore, seem to be too schematic. The periodic-flow approach has potential to serve as an alternative for a concurrent simulation. However, extensive particle separation experiments are required to really assess the quality of the particle collection predictions, as obtained with the various approaches.

Comparison with collection efficiency experiments

Hoekstra (2000) has reported on particle collection experiments in his Stairmand high-efficiency cyclone. As the solid phase, chalk dust ($CaCO_3$ powder) with a density of 2,740 $kg \cdot m^{-3}$, and a cumulative volumetric particle-size distribution as given in Figure 16, was used. He measured the overall collection efficiency $\overline{\eta}$ (the ratio between the solids mass that was collected in the dustbin and the total mass that was fed into the cyclone) for this specific powder in a cyclone with $D = 0.29$ m as a function of the inlet velocity, at three values of the exit pipe (inner) diameter. In the present numerical study only the case $D_{exit}/D = 0.5$ is considered.

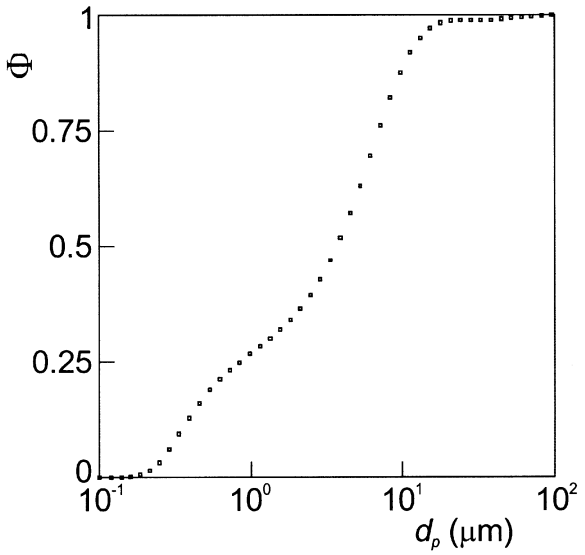

Figure 16. Cumulative volume density distribution of the $CaCO_3$ powder as used in the experiments by Hoekstra (2000).

The overall collection efficiency is related to the grade-efficiency through

$$\overline{\eta} = \int_0^1 \eta_{coll}(d_p)\, d\Phi \tag{3}$$

with $\eta_{coll}(d_p)$ the grade-efficiency as a function of the particle diameter, and Φ the cumulative volume density distribution of the powder (see Figure 16). Strictly speaking, the numerical grade-efficiency curves (Figures 12, 14, and 15) were determined for $Re = 280{,}000$, and $Fr = 90$, which in the experiments corresponds to an inlet velocity $U_{in} = 16.1$ m/s. It has been observed in the single-phase simulations, however, that the flow field (such as in terms of the profiles of the average and fluctuating velocity as presented in Figure 3) appeared to be quite insensitive of the Reynolds number (in a range $Re =$ 140,000 to 400,000). Furthermore, since centrifugal forces acting on the solid particles are much higher than gravity ($Fr \gg 1$), the influence of the specific value of the Froude number on the separation process will be weak. As a consequence, to a good approximation we may consider the numerically determined curves $\eta_{coll}(Stk)$ independent of Re and Fr. In order to evaluate the integral in Eq. 3, $\eta_{coll}(Stk)$ has to be transformed to an $\eta_{coll}(d_p)$ by means of the inlet flow velocity, the density ratio, and viscosity as applied in the experiment. In Table 1, the results of the numerically determined overall collection efficiencies (four methods) are compared to the values determined in the experiment.

Hoekstra (2000) estimates the experimental uncertainty in $\overline{\eta}$ to be of the order of 0.035. This prevents making detailed conclusions (such as rigorously falsifying one or more of the numerical methods) based on the numbers presented in Table 1. The simulated efficiencies are in fair agreement with the experimental data. The trend in the experiments ($\overline{\eta}$ increases by 0.145 when U_{in} is increased from 10 to 30 m/s) is stronger than observed in all four numerical methods. Of the latter, the trend in the concurrent simulations comes closest to the experimental result. The deviation between the concurrent and periodic-flow grade-efficiencies for the higher Stokes numbers (Figure 15) is reflected in the differences between the overall collection efficiencies of the two approaches. The Stokes number at $U_{in} = 16.1$ m/s corresponding to the mean ($d_{4,3} = 4.2$ μm) particles size in the experiment is $Stk = 1 \times 10^{-2}$.

Table 1. Overall Collection Efficiency, Experiment and Simulation

U_{in} (m/s)	$\overline{\eta}$ Exp.	$\overline{\eta}$ Concurrent Simulation	$\overline{\eta}$ Frozen-Field Simulation	$\overline{\eta}$ Eddy-Lifetime Simulation	$\overline{\eta}$ Periodic-Flow Simulation
10	0.586	0.597	0.653	0.629	0.620
16.1	—	0.643	0.689	0.669	0.663
20	0.638	0.662	0.704	0.684	0.680
30	0.731	0.692	0.728	0.710	0.708

Concluding Remarks

Results on large-eddy simulations on the single-phase flow in a Stairmand high-efficiency cyclone at $Re = 280{,}000$ show fair to good agreement with LDA data, both in terms of the average velocity, as well as in terms of the velocity fluctuations. It is worthwhile mentioning here that in order to properly calculate the flow field, the dust collector underneath the cyclone needs to be included. The flow exhibits complicated behavior, and is highly 3-D and time-dependent, due to vortex core precession: the time-averaged position of the vortex core spirals around the cyclone's geometrical center. On top of that, the core precesses in a quasi-periodic manner around its average position. The Strouhal number related to the primary frequency of the fluctuation induced by the precessing motion amounts to $S = f_{p,\mathrm{LES}} D/U_{\mathrm{in}} = 1.61$. This principal frequency is also experimentally observed, albeit that the experiment exhibits a second frequency (at $S = 0.70$) that is not resolved by the LES. The amplitude of the vortex core precession strongly depends on the axial position in the cyclone. Its maximum of 0.05 D is reached close to the entrance of the dust collection bin, that is, at the bottom of the conical section. Upon entering the vortex finder, the gas flow exhibits a vortex breakdown that forces most of the gas entering the exit pipe towards its inner wall.

In the LES flow field, solid particles of various sizes were released in an attempt to predict the separation performance of the cyclone. One-way coupling between gas and solids was assumed, and particle-particle collisions were discarded. By observing the distribution of the particle concentration as a function of the particle's Stokes numbers (dimensionless particle size) throughout the cyclone, good insight in the competition between centrifugal effects, and dispersion as a result of the turbulence, could be obtained. This competition determines if particles have a chance to reach the core region of the cyclone where they are likely to be caught in the stream towards the exit pipe. From a geometrical point of view, the complicated flow region in the top part of the cyclone (the region that contains the connection of the inlet channel to the cyclone body, as well as the vortex finder) is decisive for the separation behavior of particles slightly larger than the cut-size. A weak shortcut flow between the inlet region and vortex finder might exhaust these particles.

A concurrent simulation of gas flow and particle motion for determining grade-efficiency is a lengthy computational process since it needs to be continued until most of the particles either have been exhausted or collected. This requires the simulation of some 200 integral time scales. In an attempt to overcome this computational obstacle, three less demanding particle-motion modeling approaches have been attempted: an eddy-lifetime model, a frozen-field model, and a periodic-flow approach. In all three approaches, first gas-flow field data are gathered, and then particle motion is simulated. The first two alternatives show clear deviations (such as in terms of the cut-size and/or shape of the grade-efficiency curves) with the concurrent simulation of gas flow and particle transport. The periodic-flow approach was designed to overcome the apparently too simplifying frozen field assumption. Instead of tracking particles through a frozen field, the particles are tracked through a periodically played sequence of flow realizations, in order to let the particles feel the time-dependent character of the flow. The results in terms of grade-efficiency clearly shift towards the grade-efficiencies observed in the concurrent simulation, which makes the periodic-flow approach worthwhile exploring further. The approach requires specific choices with respect to the time interval between the subsequent flow realizations, and the time span of the sequence. The possible influence of these choices on grade-efficiency needs further investigation. Furthermore, the periodic-flow approach is cheap in terms of CPU usage, but expensive in i/o, making that a *sequential* simulation based on this approach for the specific flow system considered here took several (9) days on a Pentium III 700 MHz computer.

The amount of experimental data on collection efficiency we had to our disposal was too limited to be decisive in falsifying one or more of the numerical methods presented in this article.

Acknowledgment

The author thanks Dr. A. J. Hoekstra for making his experimental data available and for stimulating discussions on cyclonic flow.

Literature Cited

Benjamin, T. B., "Theory of the Vortex Breakdown Phenomenon," *J. Fluid Mech.*, **14**, 593 (1962).

Boysan, F., W. H. Ayers, and J. Swithenbank, "A Fundamental Mathematical Modelling Approach to Cyclone Design," *Trans. Inst. Chem. Engrs.*, **60**, 222 (1982).

Chen, S., and G. D. Doolen, "Lattice Boltzmann Method for Fluid Flows," *Annu. Rev. Fluid Mech.*, **30**, 329 (1998).

Cullivan, J. C., R. M. West, and R. A. Williams, "Efficiency-Curve Calculation for Vortex Separators," *Vortex Separation, 5th Int. Conf. on Cyclone Technologies*, L. Svarovsky and M. Thew, eds., 43, BHR Group, Cranfield, U.K. (2001).

Derksen, J. J., and H. E. A. Van den Akker, "Large-Eddy Simulations on the Flow Driven by a Rushton Turbine," *AIChE J.*, **45**, 209 (1999).

Derksen, J. J., and H. E. A. Van den Akker, "Simulation of Vortex Core Precession in a Reverse-Flow Cyclone," *AIChE J.*, **46**, 1317 (2000).

Derksen, J. J., "Assessment of Large-Eddy Simulations for Agitated Flows," *Trans. IChemE A*, **79**, 824 (2001).

Eggels, J. G. M., and J. A. Somers, "Numerical Simulation of Free Convective Flow using the Lattice-Boltzmann Scheme," *Int. J. Heat and Fluid Flow*, **16**, 357 (1995).

Escudier, M. P., J. Bornstein, and N. Zehnder, "Observations and LDA Measurements of Confined Turbulent Vortex Flow," *J. Fluid Mech.*, **98**, 49 (1980).

Escudier, M. P., J. Bornstein, and T. Maxworthy, "The Dynamics of Confined Vortices," *Proc. R. Soc. London A*, **382**, 335 (1982).

Hoekstra, A. J., J. J. Derksen, and H. E. A. Van den Akker, "An Experimental and Numerical Study of Turbulent Swirling Flow in Gas Cyclones," *Chem. Eng. Sci.*, **54**, 2055 (1999).

Hoekstra, A. J., "Gas Flow Field and Collection Efficiency of Cyclone Separators," PhD Thesis, Delft University of Technology (2000).

Hoffmann, A. C., A. van Santen, R. W. K. Allen, and R. Clift, "Effects of Geometry and Solids Loading on the Performance of Gas Cyclones," *Powder Technol.*, **70**, 83 (1992).

Hollander, E. D., J. J. Derksen, L. M. Portela, and H. E. A. van den Akker, "Numerical Scale-up Study for Orthokinetic Agglomeration in Stirred Vessels," *AIChE J.*, **47**, 2425 (2001).

Mason, P. J., and N. S. Callen, "On the Magnitude of the Subgrid-Scale Eddy Coefficient in Large-Eddy Simulations of Turbulent Channel Flow," *J. Fluid Mech.*, **162**, 439 (1986).

Métais, O., and M. Lesieur, "Spectral Large-Eddy Simulations of Isotropic and Stably Stratified Turbulence," *J. Fluid Mech.*, **239**, 157 (1992).

Ontko, J. S., "Cyclone Separator Scaling Revisited," *Powder Technol.*, **87**, 93 (1996).

Qian, Y. H., D. D'Humiéres, and P. Lallemand, "Lattice-BGK Models for the Navier-Stokes Equation," *Europhys. Lett.*, **17**(6), 479 (1992).
Schumann, U., "Subgrid Scale Model for Finite Difference Simulations of Turbulent Flows in Plane Channels and Annuli," *J. Comp. Phys.*, **18**, 376 (1975).
Slack, M. D., R. O. Prasad, A. Bakker, and F. Boysan, "Advances in Cyclone Modelling Using Unstructured Grids," *Trans IChemE*, **78A**, 1098 (2000).
Smagorinsky, J., "General Circulation Experiments with the Primitive Equations: 1. The Basic Experiment," *Mon. Weather Rev.*, **91**, 99 (1963).
Somers, J. A., "Direct Simulation of Fluid Flow with Cellular Automata and the Lattice-Boltzmann Equation," *Appl. Sci. Res.*, **51**, 127 (1993).
Spall, R. E., and B. M. Ashby, "A Numerical Study of Vortex Breakdown in Turbulent Swirling Flows," *J. Fluids Eng.*, **122**, 179 (2000).
Stairmand, C. J., "The Design and Performance of Cyclone Separators," *Trans. IChemE*, **29**, 356 (1951).

Manuscript received Apr. 1, 2002, and revision received Jan. 3, 2003.